Available online at www.sciencedirect.com
ScienceDirect
Proceedings of the Combustion Institute 31 (2007) 1533–1541
Proceedings of the Combustion Institute
www.elsevier.com/locate/proci

Experimental study of scalar filtered mass density function in turbulent partially premixed flames

Danhong Wang [a], Chenning Tong [a,*], R.S. Barlow [b], A.N. Karpetis [c]

[a] Department of Mechanical Engineering, Clemson University, Clemson, SC 29634-0921, USA
[b] Combustion Research Facility, Sandia National Laboratories, Livermore, CA 94551-0969, USA
[c] Department of Aerospace Engineering, Texas A&M Univesity, College Station, TX 77843, USA

Abstract

The mixture fraction filtered mass density function (FMDF) used in large eddy simulation (LES) of turbulent combustion is studied experimentally using line images obtained in turbulent partially premixed methane flames (Sandia flames D and E). Cross-stream filtering is employed to obtain the FMDF and other filtered variables. The means of the FMDF conditional on the subgrid-scale (SGS) scalar variance at a given location are found to vary from close to Gaussian to bimodal, indicating well-mixed and nonpremixed SGS mixing regimes, respectively. The bimodal SGS scalar has a structure (ramp–cliff) similar to the counter-flow model for laminar flamelets. Therefore, while the burden on mixing models to predict the well-mixed SGS scalar is expected to lessen with decreasing filter scale, the burden to predict the bimodal one is not. These SGS scalar structures can result in fluctuations of the SGS flame structure between distributed reaction zones and laminar flamelets, but for reasons different from the scalar dissipation rate fluctuations associated with the turbulence cascade. Furthermore, the bimodal SGS scalar contributes a significant amount of the scalar dissipation in the reaction zones, highlighting its importance and the need for mixing models to predict the bimodal FMDFs.

Keywords: Turbulent flames; Large-eddy simulation; Filtered density function; Turbulent mixing

1. Introduction

In LES of turbulent combustion the subgrid-scale (SGS) scalar mixing and the resulting instantaneous (density-weighted) distribution of scalar values in each grid volume, the filtered mass density function (FMDF), must be faithfully represented in order to predict accurately the chemical reaction rates [1–3]. An important modeling approach uses the FMDF transport equation, in which the reaction source term is in closed form, while the mixing of SGS scalars requires modeling. As a step toward understanding the mixing of multiple reactive SGS scalars and toward developing improved mixing models, the present work investigates the mixing of the SGS mixture fraction, which plays an important role in determining the mixture fraction FMDF and consequently the combustion regimes and local extinction/reignition characteristics. The FMDF is also an important model variable in several other LES approaches for nonpremixed combustion, such as the laminar flamelet method and conditional moment closure.

* Corresponding author. Fax: +1 864 6564435.
E-mail address: ctong@ces.clemson.edu (C. Tong).

1540-7489/$ - see front matter © 2006 The Combustion Institute. Published by Elsevier Inc. All rights reserved.
doi:10.1016/j.proci.2006.07.099

The current understanding of conserved scalar SGS mixing is largely based on the Kolmogorov–Obukhov–Corrsin theory, in which the SGS scalar is considered to possess certain self-similar properties. Therefore, the SGS scalar is expected to have self-similar distributions. However, our recent investigation of SGS mixing in nonreacting jets [4–7] showed, for the first time, that the SGS scalar has qualitatively different distributions and structures, depending on the instantaneous SGS scalar variance. When the SGS variance is small compared to its mean value, the SGS scalar on average has close-to-Gaussian distributions, similar to the scalar probability density function (PDF) in a fully developed scalar field, and the scalar dissipation depends weakly on the SGS scalar, indicating well-mixed SGS scalar fields. However, when the SGS variance is large compared to its mean value, the SGS scalar on average has bimodal distributions, indicating highly nonpremixed SGS scalar fields. The conditionally filtered scalar dissipation has a bell-shaped dependence on the scalar. In a nonpremixed flame such a SGS structure would indicate regions of highly segregated fuel and oxidizer separated by a sharp interface, resembling the structure of a counter-flow diffusion flame, which is a model for laminar flamelets [8]. The bimodal FDFs are similar to the scalar PDF in the early stages of binary mixing, and are contrary to the general considerations based on Kolmogorov's hypothesis.

The well-mixed and the highly nonpremixed SGS mixture fraction fields can potentially have strong influences on the flame structure. For the former the SGS scalar fluctuations at the dissipation scales (Corrsin scale, $(D^3/\epsilon)^{1/4}$) must be larger than the reaction zone width in the mixture fraction space to support laminar flamelets, where D and ϵ are the molecular diffusivity and the energy dissipation rate, respectively. This condition is similar to that given by Bilger [9]. For the bimodal SGS fields, however, the scalar value jump between the highly nonpremixed SGS regions are generally of the order of the instantaneous SGS rms value, and hence is much larger than the fluctuations predicted by the Obukhov–Corrsin scaling. Furthermore, the jump often occurs over a distance of the order of the Corrsin scale, thereby limiting the reaction zone to a layer thinner than the Corrsin length scale and resulting in laminar flamelets. This condition for laminar flamelets is similar to that given by Peters [10].

In this work, we study experimentally the SGS mixing of the mixture fraction in turbulent partially premixed flames and examine the different SGS mixture fraction distributions and structures. We investigate the characteristics of the filtered mass density function (FMDF) of the mixture fraction,

$$F_{\xi L}(\hat{\xi};\mathbf{x},t) = \langle \rho(\mathbf{x},t)\delta(\xi-\hat{\xi};\mathbf{x},t)\rangle_\ell = \int \rho(\mathbf{x}',t)\delta(\xi-\hat{\xi};\mathbf{x}',t)G(\mathbf{x}-\mathbf{x}')\mathrm{d}\mathbf{x}', \quad (1)$$

and the conditionally filtered scalar dissipation rate,

$$\langle \chi|\xi\rangle_\ell = \langle 2D\frac{\partial\xi}{\partial x_j}\frac{\partial\xi}{\partial x_j}|\xi\rangle_\ell, \quad (2)$$

which is the mixing term in the FMDF transport equation, where ξ and ρ are the mixture fraction and the fluid density, respectively. The subscripts ℓ and L denote conventional and Favre filtered variables, respectively. The filter function G is chosen to be top-hat, for which the SGS distribution (FMDF) and the (Favre) filtered mean variables can be clearly interpreted. The FMDF integrates to the filtered mixture density.

2. Experimental data

We use experimental data obtained in piloted turbulent partially premixed methane flames with a 1:3 ratio of CH_4 to air by volume (Sandia flames D and E, see Ref. [11–13]). The measurements employed combined line-imaging of Raman scattering, Rayleigh scattering, and laser-induced CO fluorescence. Simultaneous measurements of major species (CO_2, O_2, CO, N_2, CH_4, H_2O, and H_2), mixture fraction (obtained from all major species), temperature, and the radial component of scalar dissipation rate were made. The mixture fraction is calculated using a variation of Bilger's definition, which has been modified by excluding the oxygen terms [11].

The issue of measurement uncertainty was addressed in Ref. [11], which concluded that the accuracies of the measured species mass fractions, temperature, and mixture fraction are sufficient. For example, the measured values of the scalar variance in uniform calibration flows were 10^{-6} in air and 10^{-5} in flat stoichiometric flame products and in jet fluid, respectively.

The length of the imaging line is 6.0 mm with a measurement spacing of 0.2 mm. The actual measurement resolution may be larger (≈0.3 mm) due to the blurring effects of the optical system. Barlow and Karpetis (2004, 2005) addressed the issue of the spatial resolution on the measured mean scalar dissipation rate and concluded that for flame D the resolution is generally adequate beyond $x/D = 7.5$. This resolution can still under-resolve very large dissipation fluctuations, thereby under-estimating the conditionally filtered dissipation rate in cliffs. Therefore, the conclusion regarding the bimodal conditional FMDF may be slightly conservative.

Computing the FMDF and SGS variables from experimental data requires spatial filtering

of scalar fields. In this work, one-dimensional filtering is employed. While in LES the filtering is generally performed in three dimensions, our previous results have shown that the scalar filtered density function (FDF) obtained with one-dimensional filters is similar to that obtained with two-dimensional filters [4,5], which has been shown to be a very good approximation of three-dimensional filtering, with errors of approximately 5% for the rms resolvable- and subgrid-scale variables [14]. For a similar level of bimodality for the FDF, the SGS scalar variance is somewhat larger for one-dimensional filters, which are therefore expected to yield similar results. The filter sizes Δ employed in this work are 3.0 and 6.0 mm, respectively, to ensure that the results are relevant to LES, i.e., they should be significantly larger compared to the dissipative scales, allowing physics of the SGS mixing and its interaction with chemistry can be linked to inertial-range dynamics.

In our analyses 6000 line images are used at each measurement location. We use a bin width of $\Delta \ln \langle \xi''^2 \rangle = 0.34$ to ensure sufficient statistical convergence. While the precise level of statistical uncertainty is difficult to predict due to the complexity of the conditioning procedures, the degree of statistical convergence is inferred empirically using our large data set obtained in non-reacting jets [5]. We find that while the uncertainty is somewhat higher when the data size is reduced to that comparable to the current flame data, the results for the bimodal FMDF remain unchanged. Further reduction of the bin size slightly increases the bimodality of the bimodal conditional SGS scalar. Therefore, the conclusion regarding the bimodal FMDF is again somewhat conservative.

3. Results and discussions

In this section the results of the measured FMDF and the conditionally filtered dissipation are presented. Unlike a PDF and the conditional dissipation, the FMDF and the conditionally filtered dissipation are random variables, and are therefore analyzed here using their conditional averages. We use the Favre filtered mixture fraction,

$$\langle \xi \rangle_L = \langle \rho \xi \rangle_\ell / \langle \rho \rangle_\ell, \tag{3}$$

and the Favre SGS scalar variance,

$$\langle \xi''^2 \rangle_L \equiv \frac{1}{\langle \rho \rangle_\ell} \int F_{\xi L}(\hat{\xi}; \mathbf{x}, t)(\hat{\xi} - \langle \xi \rangle_L)^2 \mathrm{d}\hat{\xi} = \langle \rho \xi^2 \rangle_\ell / \langle \rho \rangle_\ell - \langle \xi \rangle_L^2 \tag{4}$$

(also random variables) as conditioning variables, which provide a measure of the unmixedness of the mixture fraction. The latter is also an important variable in the inertial-range dynamics, and therefore can relate the FMDF to the inertial-range dynamics. Such a linkage is important for modeling SGS mixing.

3.1. The conditional scalar FMDF

The conditional mixture fraction FMDF, $\langle F_{\xi L} | \langle \xi \rangle_L, \langle \xi''^2 \rangle_L \rangle$, for flame D at $x/D = 15$ for several SGS variance values is shown in Fig. 1b. The filter scale is $\Delta = 3.0$ mm and $\langle \xi \rangle_L$ is set to the stoichiometric mixture fraction, ξ_s (=0.35), to maximize the probability of the SGS field containing reaction zones. For small SGS variance, e.g. $\langle \xi''^2 \rangle_L \approx 0.0004$, the conditional FMDF is unimodal and generally not far from Gaussian. Such a distribution is similar to those obtained in nonreacting flows and to the scalar PDF in a fully developed turbulent flow, indicating that the SGS mixture fraction is well mixed. Previous results [4,5] have shown that the SGS scalar under such conditions is in spectral equilibrium, suggesting

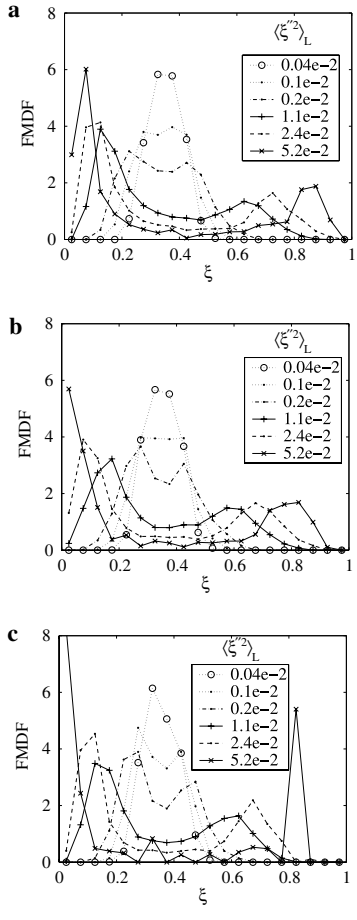

Fig. 1. Conditional FMDF in flame D for $\Delta = 3.0$ mm and $\langle \xi \rangle_L = 0.35$. (a) $x/D = 7.5$; (b) $x/D = 15$; (c) $x/D = 30$.

that the SGS scalar is consistent with Kolmogorov's cascade picture. Therefore, the average SGS scalar fluctuations decreases with the filter scale, suggesting that the burden on the SGS mixing models is lessened.

As the SGS variance increases, the FMDF becomes bimodal, with the bimodality stronger for larger SGS variance, indicating that the rich and lean mixtures in the SGS field (i.e., a grid cell) are essentially segregated. Furthermore, there is a sharp interface (diffusion-layer) separating the two regions, across which there is a large scalar value jump (see the discussion on the conditionally filtered scalar dissipation rate below). This SGS scalar structure is essentially a ramp–cliff structure (see Ref. [15]), with the rich and lean mixtures forming the ramps and the diffusion layer as the cliff. The bimodal FMDF is also similar to the scalar FDF for large SGS variance observed in nonreacting flows [4]. Our previous results also showed that the SGS scalar with a large variance is in spectral nonequilibrium, which, along with the presence of the ramp–cliff structure, suggests that the bimodal SGS scalar is not well described by Kolmogorov's turbulence cascade picture. Because the ramp–cliff structure exists in the subgrid scales for all filter sizes significantly larger than the Corrsin scale, as is the case in most LES, the burden on mixing models to capture the bimodal FMDF does not lessen with decreasing filter scale.

The value of the Favre filtered mixture fraction has different effects on the unimodal and bimodal conditional FMDFs. For a unimodal FMDF, the shape remains approximately unchanged when $\langle\xi\rangle_L$ increases from 0.35 to 0.45 (Fig. 2a), but the position of the peak shifts rightward to approximately 0.42 (leftward to 0.22 for $\langle\xi\rangle_L = 0.25$, not shown). The close-to-Gaussian distributions indicate that the conditional SGS mixture fraction fields are still well-mixed and diffuse toward $\langle\xi\rangle_L$. For $\langle\xi\rangle_L$ values sufficiently away from ξ_s, the SGS field might not contain any reaction zones. Therefore, the FMDFs of such fields are of less interest and not shown. For a bimodal FMDF, the positions of the two peaks move much less than that of a unimodal FMDF as $\langle\xi\rangle_L$ increases, but with the left and right peak values decreasing and increasing respectively, reflecting the increase in the $\langle\xi\rangle_L$ value. This result indicates that variations of the $\langle\xi\rangle_L$ value only alter the fraction of the fuel-lean region relative to that of the fuel-rich region in the conditionally sampled SGS field.

The conditional FMDFs at different downstream locations (Fig. 1) exhibit similar characteristics to that at $x/D = 15$. The maximum value of the conditional SGS mixture fraction decreases somewhat with increasing downstream distance. Far downstream the maximum will be significantly less than unity (no pure fuel left). However, the qualitative characteristics of close-to-Gaussian and bimodal distributions are expected to remain the same, as observed in non-reacting jets[4,16].

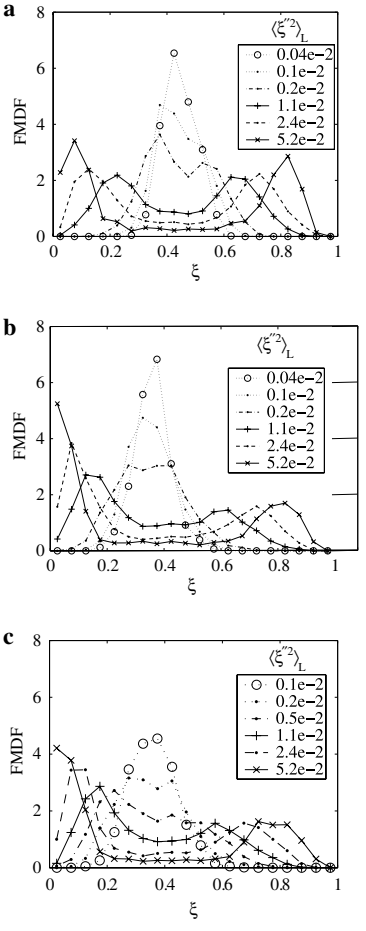

Fig. 2. Conditional FMDF at $x/D = 15$. (a) Flame D, $\Delta = 3.0$ mm, $\langle\xi\rangle_L = 0.45$; (b) flame D, $\Delta = 6.0$ mm, $\langle\xi\rangle_L = 0.35$; (c) flame E, $\Delta = 3.0$ mm, $\langle\xi\rangle_L = 0.35$.

The filter scale is an important parameter in LES and it is important to understand how the FMDF varies with it. The results for the two filter scales (3.0 and 6.0 mm) at $x/D = 15$ (Figs. 1b and 2b) are very similar, further demonstrating that the bimodal FMDF is an inherent property of the SGS scalar with large SGS variance and that the burden on the mixing model to predict the bimodal distributions does not lessen with decreasing filter scale. The results also show that the transition from unimodal to bimodal FMDF for the two filter scales (defined here as the point at which the top of the FMDF becomes flat) occurs at approximately $\langle\xi''^2\rangle_L = 0.001$ and 0.002, respectively. This difference is related to the mean SGS variance for $\Delta = 3.0$ mm (0.0025) being smaller than that for $\Delta = 6.0$ mm (0.0034).

Previous results [4,16] have shown that in the fully developed region of a non-reacting jet the scalar FDF essentially can be collapsed by the normalized SGS variance, $\langle \xi''^2 \rangle_L / \langle \xi''^2 \rangle$, regardless of the filter size (as long as it is sufficiently large compared to the Corrsin scale). The results in Figs. 1b and 2b are qualitatively consistent with the previous results. However, in a developing flow this might not be true. Comparing Fig. 1a and b we find that in both cases the transition to bimodal FMDF occurs approximately at $\langle \xi''^2 \rangle_L = 0.001$, although the mean values of the SGS variance differ by nearly a factor of 2 (0.0065 vs 0.0034). These results might be because the turbulence is evolving rapidly near the nozzle.

The FMDF results show that the statistical structure of the SGS mixture fraction is qualitatively different for small and large SGS variance values. For a bimodal FMDF, the difference between the ξ values for its peaks is often larger than the near-equilibrium (or mildly strained flamelets) reaction zone width in the ξ space for these methane flames, $\Delta\xi_R$ ($\approx$0.23), defined by the lean and rich limits that correspond to 10% of the peak CO oxidation reaction rate in laminar flames [17]. Therefore, such a mixture fraction structure is likely to limit the reaction zones in thin diffusion layers, thereby resulting in laminar flamelets. By contrast, for the well-mixed SGS mixture fraction field, the turbulence cascade is likely to dominate and the dissipation-scale scalar fluctuations largely follow the Kolmogorov–Obukhov–Corrsin predictions. Therefore, such a SGS scalar is likely to result in distributed reaction zones.

3.2. The conditionally filtered scalar dissipation

The conditionally filtered scalar dissipation, $\langle\langle \chi|\xi\rangle_\ell|\langle\xi\rangle_L, \langle\xi''^2\rangle_L\rangle$, for the same conditions as Fig. 1 is shown in Fig. 3. Similar to the FMDF, $\langle \chi|\xi\rangle_\ell$ also has qualitatively different functional forms for small and large SGS variance. For small $\langle \xi''^2 \rangle_L$ it shows a weak dependence on ξ, consistent with the conditional FMDF being unimodal and not far from Gaussian, providing further evidence that the SGS mixture fraction is well-mixed. For large $\langle \xi''^2 \rangle_L$, the conditionally filtered dissipation becomes bell-shaped, with the maximum value increasing with the SGS variance value. Furthermore, the maximum value occurs at the ξ value where the bimodal FMDF has the minimum, indicating that there is a sharp interface between the highly segregated SGS mixture fraction regions, which is essentially a diffusion layer (cliff) with a thickness of the order of the Corrsin scale. Because the diffusion is toward the scalar value at the center of the diffusion layer (cliff), independent of the chemistry, mixing models such as the interaction by exchange with the mean (IEM) model can lead to unphysical mixing across ξ_s (the reaction zone).

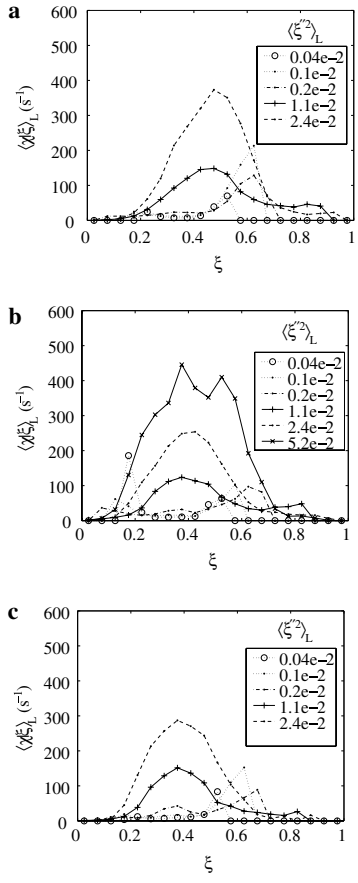

Fig. 3. Conditionally filtered scalar dissipation, $\langle\langle \chi|\xi\rangle_\ell|\langle\xi\rangle_L, \langle\xi''^2\rangle_L\rangle$, in flame *D*. Conditions same as in Fig. 1.

The FMDF and the conditionally filtered dissipation results suggest that the SGS mixture fraction structure under the condition of large SGS variance is similar to that in the counter-flow model for laminar flamelets. However, Rajagopalan and Tong [16] noted that the lean and rich mixtures in a bimodal SGS scalar generally do not have ξ values of 0 and 1 respectively, a situation similar to that noted by Bish and Dahm [18]. Therefore, the laminar flamelets resulted are not simple flamelets obtained using $\xi = 0$ and 1 as boundary conditions. The FMDF results show that the boundary conditions for these flamelets are essentially the ξ values for the two FMDF peaks.

The observed relationship between the scalar FMDF and conditionally filtered dissipation for small and large SGS variance is also similar to that between the scalar PDF and the conditional dissipation [4,5]. This is remarkable because while the scalar PDF and the conditional dissipation are related through the scalar PDF equation, there is

no analogous equation relating the conditional FMDF and the conditionally filtered dissipation. Therefore, the relationship suggests that the dynamics of the conditional SGS fields are very similar to fully developed and rapidly evolving scalar fields, respectively. The similarities between the above results and those obtained in nonreacting flows also suggest that heat release does not change qualitatively the structure of the SGS mixture fraction fields, although other aspects of the SGS scalar may still be influenced by heat release.

The conditionally filtered dissipation at $x/D = 15$ for the larger filter scale $\Delta = 6.0$ mm in Fig. 4b. has similar characteristics to those for $\Delta = 3.0$ mm, but the maximum value is much lower for the same large SGS variance value. For example, for $\langle\xi''^2\rangle_L = 0.052$, the maximum value of $\langle\chi|\xi\rangle_\ell$ is above 400 s^{-1} for $\Delta = 3.0$ mm while it is only near 150 s^{-1} for $\Delta = 6.0$ mm. We argue that this difference is due to two factors. First, the transition from unimodal to bimodal FMDF occurs at a smaller SGS variance value for $\Delta = 3.0$ mm (Figs. 1b and 2b). Therefore, we expect that for a given SGS variance, the bimodality is stronger, and therefore the dissipation is higher. Second, because of the relatively low Reynolds number of the flame, the filter sizes employed are not very large compared to the scalar dissipation scales (≈0.5 mm in cliffs). Consequently, for the same SGS variance value, the average width of the diffusion layer sampled must be smaller in when the filter size decreases, resulting in a higher in-layer dissipation rate.

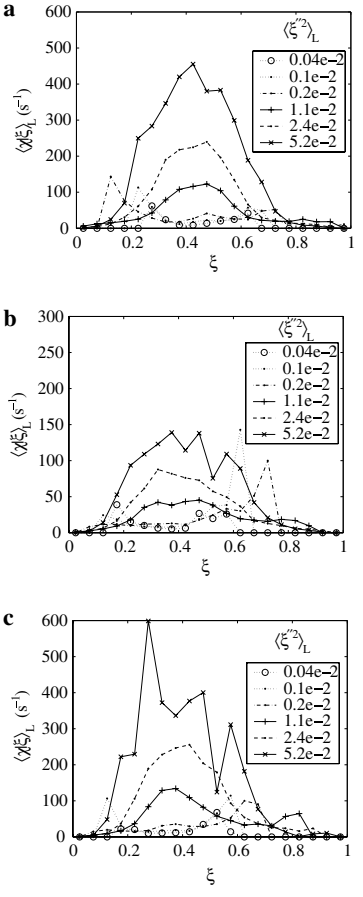

Fig. 4. Conditionally filtered scalar dissipation, $\langle\langle\chi|\xi\rangle_\ell|\langle\xi\rangle_L, \langle\xi''^2\rangle_L\rangle$. Conditions same as in Fig. 2.

The conditionally filtered dissipation for $\langle\xi\rangle_L = 0.45$ (Fig. 4a) has similar functional forms to those for $\langle\xi\rangle_L = 0.35$, in contrast with the larger changes in the FMDF, especially for large SGS variance values. Because the peak region of the conditionally filtered dissipation is dominated by the cliff, its weaker dependence on $\langle\xi\rangle_L$ indicates that essentially the same cliff is captured by the conditional sampling procedure. The ramps are sampled differently (see Fig. 2a for FMDF), but they correspond to much lower dissipation values, and therefore do not affect the overall functional form of $\langle\chi|\xi\rangle_\ell$.

Comparisons among the results for the conditionally filtered dissipation at the three downstream locations (Fig. 3) show that the maximum value for $\langle\chi|\xi\rangle_\ell$ with large SGS variance decreases from $x/D = 7.5$ to 15, which is due to two reasons. First, the dissipation length scale generally increases with the downstream distance, resulting in a larger diffusion layer thickness and a smaller $\langle\chi|\xi\rangle_\ell$. Second, for large SGS variance there are extinction events at $x/D = 15$ compared to nearly no extinction at $x/D = 7.5$ [19], thereby reducing the scalar diffusivity, and consequently the conditionally filtered dissipation. From $x/D = 15$ to 30 the dissipation length scale further increases, which tends to reduce the $\langle\chi|\xi\rangle_\ell$. However, most extinguished fluid parcels have reignited at this location, which tend to increase $\langle\chi|\xi\rangle_\ell$. Due to these competing effects, the maximum value for the conditional $\langle\chi|\xi\rangle_\ell$ at $x/D = 30$ increases slightly compared to that at $x/D = 15$.

The results for the conditional FMDF (Fig. 2c) and $\langle\chi|\xi\rangle_\ell$ (Fig. 4c) for flame E are similar to those for flame D. The jet velocity is higher in flame E, resulting in higher strain rates and more local extinction events. The higher strain rates tend to result in higher scalar dissipation rates. In addition, local extinction may lead to stronger entrainment since heat release tends to suppress entrainment [20], thereby enhancing the dissipation in cliffs. However, local extinction also tends to reduce the diffusivity and dissipation. Moreover, the higher Reynolds number and possibly the local extinction reduce the local scalar dissipation length scale, potentially resulting in insufficient measurement resolution and lower measured dissipation rate. Probably as a result of these competing effects, the maximum value

for $\langle\chi|\xi\rangle_\ell$ for flame E (Fig. 4c) is approximately equal to (or slightly smaller than) that for flame D. Further understanding of the effects may require measurements of flame E at a higher resolution.

The above results indicate that the SGS mixture fraction fields have different spatial structures for small and large SGS variance values. We provide in Fig. 5 several examples of conditional SGS mixture fraction and mixture fraction-scalar dissipation profiles. For small SGS variance, the $\chi-\xi$ profiles have no clear structures, consistent with the well-mixed SGS mixture fraction. The rms (the instantaneous standard deviation) and dissipation-scale SGS mixture fraction fluctuations are smaller than the reaction zone width $\Delta\xi_R$ ($\approx$0.23). The measured scalar dissipation values (even after multiplying them by a factor of three using the assumption of local isotropy) are smaller than the extinction dissipation rate for a steady laminar flame ($\chi_q = 400\ s^{-1}$ for the fuel considered), indicating that the conditional SGS flame is in the form of quasi-equilibrium distributed reaction zones. For large SGS variance, the SGS ξ profiles show large jumps in mixture fraction (the cliff), effectively limiting the reaction zone to within the structure and resulting in laminar flamelets. The $\chi-\xi$ profiles are also consistent with this structure. For several profiles the dissipation (even one component) exceeds the extinction value. Therefore, the local extinction events under such conditions are most likely in the form of flamelet extinction.

The results also suggest that at a given location in a turbulent flame, the SGS reaction zones fluctuate between distributed reaction zones and laminar flamelets due to the occurrences of the well mixed and highly nonpremixed SGS mixture fraction fields. This cause for the occurrences of both flame structures is different from previous arguments based on the fluctuations in the scalar dissipation rate due to the turbulence cascade. The scalar dissipation rate at a point, by itself, does not provide sufficient information about the structure of the local mixture fraction field. The variations of the flame structure with the SGS mixture fraction structure suggest that mixing models need to be able to capture the well-mixed and bimodal distributions to account for these flame structures.

To further understand the impact of the SGS mixture fraction structure on the flame structure, it is important to quantify the potential contributions to the heat release from each type of flame structure. We first quantify the portion of the SGS fields containing ramp–cliff structures by plotting the PDF of $\ln\langle\xi''^2\rangle_L$ in flame D at $x/D = 15$ (Fig. 6). The PDFs are approximately log-normally distributed with the peaks located at about $\langle\xi''^2\rangle_L = 0.0067$ and 0.014, respectively. The conditional FMDF (Fig. 1b) is already bimodal for the $\langle\xi''^2\rangle_L$ values at the peak location of the $\ln\langle\xi''^2\rangle)_L$ PDF, indicating that well over 30% of the SGS scalar field contains ramp–cliff

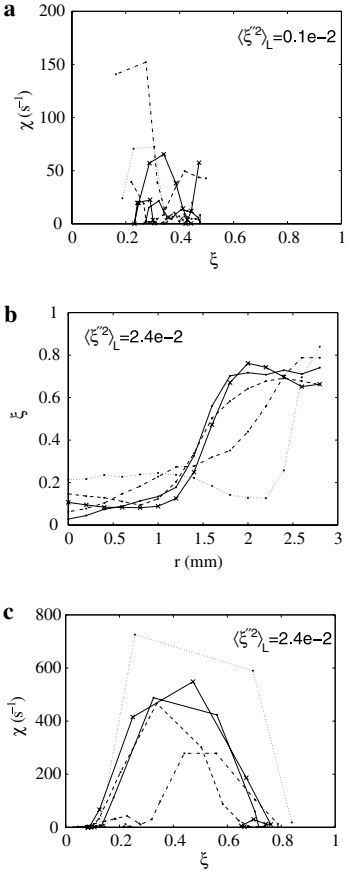

Fig. 5. Conditional profiles in flame D for $\langle\xi\rangle_L = 0.35$. $x/D = 15$, $\Delta = 3.0$ mm. (a) and (c) $\chi-\xi$; (b) ξ.

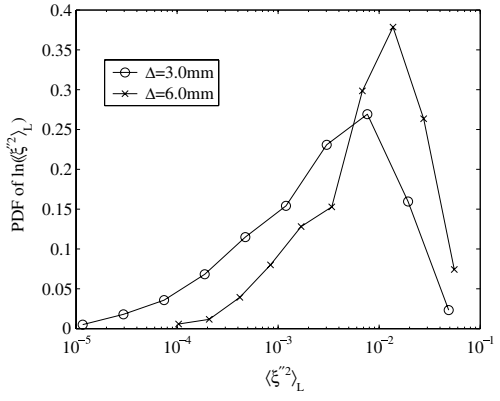

Fig. 6. PDF of $\ln(\langle\xi''^2\rangle_L)$ in flame D at $x/D = 15$. $\langle\xi\rangle_L = 0.35$.

Table 1
Contributions to the scalar dissipation rate from the ramp–cliff structure ($\langle\xi''^2\rangle_L > V$) within the reaction zone for different V values

Flame	Δ (mm)	V				
		0.001	0.002	0.005	0.011	0.024
D	3.0	0.879	0.739	0.527	0.254	0.049
D	6.0	0.981	0.934	0.815	0.532	0.189
E	3.0	0.851	0.69	0.451	0.182	0.026
E	6.0	0.97	0.901	0.731	0.41	0.102

structures ($\langle\xi''^2\rangle_L > 0.005$ and 0.01 for $\Delta = 3$ and 6 mm, respectively). These results are essentially independent of the chemistry. Among these SGS fields, only those containing scalar value jumps larger than $\Delta\xi_R$ can result in laminar flamelets.

To quantify the potential contributions to the heat release from the bimodal SGS fields, which is chemistry (reaction zone width) dependent, we calculate the ratio of the contributions to the scalar dissipation rate from the portion of the ramp–cliff structure where the reaction zone resides ($\xi_s - \frac{\Delta\xi_R}{2} < \xi < \xi_s + \frac{\Delta\xi_R}{2}$) to those from all the reaction zones as,

$$\frac{\int_V^\infty \int_{\xi_s-\frac{\Delta\xi_R}{2}}^{\xi_s+\frac{\Delta\xi_R}{2}} \langle\langle\chi\delta(\xi-\hat{\xi})\rangle_L|\langle\xi''^2\rangle_L\rangle P_{\langle\xi''^2\rangle_L} \mathrm{d}\hat{\xi}\mathrm{d}\langle\xi''^2\rangle_L}{\int_{\xi_s-\frac{\Delta\xi_R}{2}}^{\xi_s+\frac{\Delta\xi_R}{2}} \langle\chi\delta(\xi-\hat{\xi})\rangle \mathrm{d}\hat{\xi}}, \tag{5}$$

because heat release is, to the first order approximation, proportional to the scalar dissipation rate, where $P_{\langle\xi''^2\rangle_L}$ is the PDF of $\langle\xi''^2\rangle_L$. The results for several V values are given in Table 1. For both filter scales the scalar dissipation for large SGS variance ($\langle\xi''^2\rangle_L > 0.005$ and 0.01, respectively) accounts for more than 50% of the total scalar dissipation within the reaction zones, suggesting that a significant amount of the heat release comes from the ramp–cliff structure, although it only occupies a small fraction of the spatial volume. These results indicate that bimodal SGS mixture fraction associated with the ramp–cliff structure and the resulting laminar flamelets play important roles in nonpremixed/partially premixed flames and must be properly accounted for by mixing models.

4. Conclusions

We use data obtained in turbulent partially premixed flames (Sandia flames *D* and *E*) to study the SGS mixing of mixture fraction. The Favre filtered mixture fraction and the Favre SGS scalar variance are used as conditioning variables for analyzing the scalar FMDF and the conditionally filtered scalar dissipation.

The results show that for small SGS scalar variance, the FMDF is unimodal regardless of the filter scale, the measurement location, and the filtered mixture fraction value. However, the peak position of the FMDF shifts with the filtered mixture fraction. The conditionally filtered scalar dissipation rate depends weakly on the SGS scalar, indicating that the SGS scalar is well mixed and the turbulence cascade is likely to dominate the SGS mixing process. Therefore, such a SGS mixture fraction is likely to result in distributed reaction zones.

For large SGS variance, however, the FMDF becomes bimodal and the conditionally filtered scalar dissipation is bell-shaped, indicating the existence of a ramp–cliff structure, which is similar to the mixture fraction profile in the counter-flow model for laminar flamelets. The mixture fraction structure captured does not depend on the filtered mixture fraction value. For the measurement locations considered the difference in mixture fraction values for the two FMDF peaks are generally larger than the reaction zone width in the mixture fraction space, therefore the SGS mixing field under such conditions support flamelets. These findings are similar to our previous results obtained in nonreacting jets, indicating that heat release does not alter the qualitative characteristics of the SGS mixture fraction fields.

These results suggest that at a given location the SGS flame fluctuates between distributed reaction zones and laminar flamelets, but for reasons different from previous arguments based on scalar dissipation fluctuations resulted from the turbulence cascade. The strong effects of the bimodal SGS scalar on the flame structure indicate that mixing models need to be able to capture its distributions to account for the different flame structures. The results for the contributions to the heat release from bimodal SGS fields suggest that a significant amount of heat release comes from the ramp–cliff structure, further highlighting its importance in flames and the need for mixing models to capture the bimodal FMDF.

The results for the FMDF with two filter sizes suggest that or small SGS variance, the burden on the SGS mixing models lessens with decreasing filter scale because the SGS scalar is likely to follow the Kolmogorov's cascade picture. For larger SGS variance, large scalar value jumps exist in the SGS scalar for all filter scales significantly larger than the Corrsin scale, therefore the burden on the mixing model does not lessen with decreasing filter size.

Acknowledgments

The work at Clemson was supported by the Air Force Office of Scientific Research under Grant FA9550-06-1-0036 (Dr. Julian M. Tishkoff,

program manager) and by the National Science Foundation under grant CTS-0093532 (CAREER award). The work at Sandia was supported by the Division of Chemical Sciences, Geosciences, and Biosciences, the Office of Basic Energy Sciences, the U.S. Department of Energy. We thank Professor Stephen B. Pope for reading the draft paper and providing valuable comments.

References

[1] S.B. Pope, *Proc. Combust. Inst.* 23 (1990) 591–612.
[2] P.J. Colucci, F.A. Jaberi, P. Givi, S.B. Pope, *Phys. Fluids* 10 (1998) 499–515.
[3] M. Sheikhi, T. Drozda, P. Givi, F. Jaberi, S. Pope, *Proc. Combust. Inst.* 30 (2005) 549–556.
[4] C. Tong, *Phys. Fluids* 13 (2001) 2923–2937.
[5] D. Wang, C. Tong, *Phys. Fluids* 14 (2002) 2170–2185.
[6] D. Wang, C. Tong, S.B. Pope, *Phys. Fluids* 16 (2004) 3599–3613.
[7] D. Wang, C. Tong, *Proc. Combust. Inst.* 30 (2005) 567–574.
[8] N. Peters, *Prog. Eng. Combust. Sci.* 10 (1984) 319–339.
[9] R.W. Bilger, *Proc. Combust. Inst.* 22 (1988) 475–488.
[10] N. Peters, *Turbulent Combustion*, Cambridge University press, Cambridge, England, 2000.
[11] R.S. Barlow, A.N. Karpetis, *Flow, Turb. Combust.* 72 (2004) 427–448.
[12] A.N. Karpetis, R.S. Barlow, *Proc. Combust. Inst.* 30 (2005) 665–672.
[13] R.S. Barlow, A.N. Karpetis, *Proc. Combust. Inst.* 30 (2005) 673–680.
[14] C. Tong, J.C. Wyngaard, S. Khanna, J.G. Brasseur, *J. Atmos. Sci.* 55 (1998) 3114–3126.
[15] C. Tong, Z. Warhaft, *Phys. Fluids* 6 (1994) 2165–2176.
[16] A.G. Rajagopalan, C. Tong, *Phys. Fluids* 15 (2003) 227–244.
[17] J.H. Frank, S.A. Kaiser, M.B. Long, *Proc. Combust. Inst.* 29 (2002) 2687–2694.
[18] E.S. Bish, W.J.A. Dahm, *Combust. Flame* 100 (1995) 457–464.
[19] D. Wang, Ph.D. dissertation, Clemson University, Department of Mechanical Engineering (July 2005).
[20] A.N. Karpetis, R.S. Barlow, *Proc. Combust. Inst.* 29 (2002) 1929–1936.